

Tug-of-war as a cooperative mechanism for bidirectional cargo transport by molecular motors.

- Supporting Information (SI) -

Melanie J.I. Müller^{*}, Stefan Klumpp[†], and Reinhard Lipowsky^{‡*}

^{*}Max Planck Institute of Colloids and Interfaces, Science Park Golm, 14424 Potsdam, Germany, and [†]Center for Theoretical Biological Physics, University of California San Diego, La Jolla, CA 92093-0374, USA

Model for a single motor. A single motor can walk along a MT with velocity v , unbind from the MT with unbinding rate ϵ and bind to the MT with binding rate π . Our choice of the rates is based on the load-dependent transport parameters of single motors as measured in single-molecule experiments. When bound to the MT, the motor moves forward with a load-dependent velocity which decreases monotonically from the zero-load forward velocity v_F to zero at the stall force F_s [1, 2, 3, 4]. For superstall loads the motor walks slowly backwards, as has been shown for kinesin [2, 5]. In our model, we used a piecewise linear force-velocity relation with

$$v(F) = \begin{cases} v_F (1 - F/F_s) & \text{for } F \leq F_s \\ v_B (1 - F/F_s) & \text{for } F \geq F_s \end{cases} \quad [1]$$

Here, v_B is the absolute value of the motor backward velocity. For forces smaller than the stall force, such a linear relation provides a good approximation for the experimentally determined force-velocity curves both for kinesin [1, 2, 3] and dynein [4]. For superstall forces, the shape of the force-velocity curve is not known precisely. In this range our linear relation can be considered as a Taylor expansion to first order in $F - F_s$. The detailed form of the force-velocity curve is however not crucial for our results, as long as it decreases monotonously and exhibits a small backward velocity. The unbinding rate of the motor from the MT increases exponentially with the applied force F :

$$\epsilon(F) = \epsilon_0 \exp(|F|/F_d) \quad [2]$$

as measured for kinesin [1] and as follows from Kramers or Bell theory. The force scale is set by the detachment force F_d . The binding rate to the MT is difficult to assess experimentally. It is expected to depend only weakly on the load because an unbound motor relaxes and then binds from its relaxed state (see the discussion in [6]). We therefore take the binding rate equal to the zero-load binding rate π_0 , independent of load:

$$\pi(F) = \pi_0 \quad [3]$$

The single motor rates of kinesin 1, cytoplasmic dynein and an unknown plus motor that transports lipid-droplets in *Drosophila* embryos are shown in Table 1. For kinesin 1 all parameters have been measured in single-molecule experiments, see the references in the table. For dynein, only part of the parameters have been measured, and for the stall force conflicting results have been reported by different labs, see the references given in Table 1. In addition, dynein is very sensitive to regulatory and accessory proteins [7]. The unknown dynein parameters and the parameters of the unknown *Drosophila* plus motor are obtained by fitting experimental data from *Drosophila* droplet transport [8, 9, 10] as described in the section 'Fit to the lipid-droplet data' below.

Effective rates for the cargo. We consider a cargo that is transported by constant numbers of N_+ plus and N_- minus motors. At every time t , the state of the cargo with N_+ plus and N_- minus motors firmly attached to it is fully characterized by the numbers n_+ and n_- of plus and minus motors that are bound to the MT and thus actively pull on the cargo at that time. The state of the cargo changes when a plus or a minus motor binds or unbinds to/from the MT, see Fig. 2. These changes are described by a Master equation for the probability distribution $p(n_+, n_-, t)$ to have n_+ bound plus and n_- bound minus motors at time t . The rates of this Master equation describe the transitions corresponding to the arrows in Fig. 2 and are determined from the single-motor rates using the assumptions that the motors act independently and feel each other only due to two effects: (i) opposing motors act as load, and (ii) identical motors share this load. If each plus motor feels the load F_+ (and generates the force $-F_+$) and each minus motor feels the load $-F_-$ (and generates the force F_-), this means that the force balance on a cargo pulled by n_+ plus and n_- minus motors is

$$n_+ F_+ = -n_- F_- \equiv F_c. \quad [4]$$

Here, the sign of the force is chosen positive if it is a load on the plus motors, i.e. if it points into the minus direction. If only one motor type is bound, i.e. if $n_+ = 0$ or $n_- = 0$, then $F_+ = F_- = F_c = 0$. A single bound plus motor thus feels the force $F_+ = F_c/n_+$. Using Eqs. [2] and [3], this implies that the effective rate for the unbinding of one plus motor is

$$n_+ \epsilon_{0+} \exp[F_c/(n_+ F_{d+})], \quad [5]$$

and the effective rate for the binding of one plus motor is

$$(N_+ - n_+) \pi_{0+}. \quad [6]$$

Here and in the following, the index '+' labels plus motor properties. Analogous expressions hold for the minus motors with the parameters indexed by '-'.

The cargo force F_c is determined by the condition that plus motors, which experience the force F_c/n_+ , and minus motors, which experience the force $-F_c/n_-$, move with the same velocity, which is the cargo velocity v_c :

$$v_c(n_+, n_-) = v_+(F_c/n_+) = -v_-(-F_c/n_-) \quad [7]$$

Here, the sign of the velocity is taken positive in the plus direction and negative in the minus direction. In order to have a unique solution F_c to this equation, both motors must have nonzero backward velocities; otherwise the single-motor force velocity relations $v_+(F)$ and $v_-(F)$ do not have well-defined inverses. In the case of 'stronger plus motors'

[‡]To whom correspondence should be addressed. E-mail: lipowsky@mpikg.mpg.de

©2008 by The National Academy of Sciences of the USA

$n_+F_{s+} > n_-F_{s-}$, Eqs. [1] and [7] lead to the cargo force and velocity

$$F_c(n_+, n_-) = \lambda n_+F_{s+} + (1 - \lambda)n_-F_{s-} \quad [8]$$

$$v_c(n_+, n_-) = \frac{n_+F_{s+} - n_-F_{s-}}{n_+F_{s+}/v_{F+} + n_-F_{s-}/v_{B-}} \quad [9]$$

with $\lambda = 1/(1 + (n_+F_{s+}v_{B-})/(n_-F_{s-}v_{F+}))$. The cargo moves to the plus direction, $v_c > 0$. In the opposite case of 'stronger minus motors' with $n_+F_{s+} < n_-F_{s-}$, in Eqs. [8] and [9] the plus motor forward velocity v_{F+} has to be replaced by its backward velocity v_{B-} , and the minus motor backward velocity v_{B-} by its forward velocity v_{F-} . The cargo moves into the minus direction, $v_c < 0$. Typically the backward velocity is rather small, so that a cargo with $n_+, n_- > 0$ pulled by both types of motors usually moves very slowly, as indicated by the 'blockade' situation in Fig. 1(0). If however only one motor type is bound, e.g. if $n_- = 0$, the cargo moves fast with the single plus motor velocity $v_c = v_{F+}$, corresponding to Fig. 1(+).

Eqs. [5], [6], [8], and the corresponding equations for minus motors, fully determine the rates that enter the Master equation for the motor number probability $p(n_+, n_-, t)$ on the state space $0 \leq n_+ \leq N_+$, $0 \leq n_- \leq N_-$. In each state (n_+, n_-) , the cargo moves with velocity $v_c(n_+, n_-)$ as given by Eq. [9].

Experiments usually observe only cargos that have been bound to the MT for an unknown time period and monitor them over a timescale of minutes which is large compared to the timescales of motor (un-)binding, which are of the order of seconds. We are therefore interested in the long-time behaviour of the cargo which corresponds to the time-independent steady state solution $p(n_+, n_-)$ of the Master equation.

External forces. If an external force F_{ext} is present, the force balance Eq. [4] becomes

$$n_+F_+ = -n_-F_- + F_{\text{ext}}. \quad [10]$$

Here again, forces are taken to be positive if they point into the minus direction. Carrying through the same calculation as for the case without external force leads to the velocity of a cargo transported into the plus direction by n_+ active plus and n_- active minus motors under an opposing external force F_{ext} :

$$v_c(n_+, n_-, F_{\text{ext}}) = \frac{n_+F_{s+} - n_-F_{s-} - F_{\text{ext}}}{n_+F_{s+}/v_{F+} + n_-F_{s-}/v_{B-}} \quad [11]$$

In the case of minus motion under an opposing force F_{ext} (which is then negative), the plus motor forward velocity v_{F+} has to be replaced by its backward velocity v_{B-} , and the minus motor backward velocity v_{B-} by its forward velocity v_{F-} .¹ Thus the stall force of a cargo pulled by n_+ plus and n_- minus motors is given by

$$F_{s,c}(n_+, n_-) = n_+F_{s+} - n_-F_{s-}, \quad [12]$$

as intuitively expected.

Numerical calculations. For a given set of single-motor parameters, we numerically calculate the steady state solution $p(n_+, n_-)$ as the nullspace of the transition matrix of the Master equation [11]. Such motor number probabilities are shown in Fig. 3A2-C2 and Fig. 4A2-C2. We then determine the

locations $(\tilde{n}_+, \tilde{n}_-)$ of maxima of $p(n_+, n_-)$ which define the 'motility state' of the cargo. $p(\tilde{n}_+, \tilde{n}_-)$ is a maximum if it is larger than its direct and diagonal neighbours on the state space (n_+, n_-) . A maximum at a state $(\tilde{n}_+, 0)$ with $\tilde{n}_+ > 0$ corresponds to a plus motion state labeled by '+', a maximum at $(0, \tilde{n}_-)$ with $\tilde{n}_- > 0$ to a minus motion state labeled by '-', and a maximum at a state $(\tilde{n}_+, \tilde{n}_-)$ with both \tilde{n}_+ and \tilde{n}_- larger than zero to a no-motion state labeled by '0'. For a given set of single-motor parameters, there is at most one of each type of maximum. Thus there are seven possible combinations of maxima, which give the seven motility states (+), (-), (0), (0+), (-0), (-+), and (-0+). In the motility state (0+), for example, there are two maxima, one at a plus-motion state $(\tilde{n}_+, 0)$, and one at a no-motion state $(\tilde{n}_+, \tilde{n}_-)$. If the probability maximum is at (0, 0), the cargo is in the 'unbound' state.

In order to obtain dynamical quantities such as trajectories, run lengths and run velocities, we generate individual cargo trajectories using the Gillespie algorithm [12] for the binding/unbinding dynamics and let the cargo move with the velocity v_c in the intervals between binding/unbinding events. At the start of the simulation, a cargo is bound to the filament by a random number of n_+ active plus and n_- active minus motors. In order to suppress transient behavior due to initialization bias, measurement of run lengths and velocities is started only after a time lapse of 10^4 s. The obtained velocity and run length distributions as shown in Fig. 3A3-C3, Fig. 4A3-C3 and Fig. 5A, and all average values, are obtained from 20-50 trajectories, each of which lasts 10^6 s.

For comparison with experiments, the analysis of the simulated trajectories is performed in close analogy with the analysis of the experimental trajectories of [8, 9, 10]. The cargo displacement (as shown in Fig. 3A2-C2 and Fig. 4A2-C2) is recorded at video frequency of 30/s. The obtained trajectories are segmented into runs and pauses by using the definitions from [9, 10]: A cargo is considered to be moving into the plus (minus) direction if its velocity v_c is larger than 50 nm/s (smaller than -50 nm/s) and pausing else. A run has to be at least 30 nm and 0.16 s long, and a pause must be longer than 0.23 s and cover a distance smaller than 30 nm. The run velocity is defined as the ratio of run length and run time.

Motility diagrams. In the symmetric tug-of-war, for which the number of plus and minus motors are the same and for which plus and minus motors have identical single-motor parameters except for their preferred direction of motion, the cargo motion depends on four dimensionless parameters: the number $N = N_+ = N_-$ of plus and minus motors, the stall force to detachment force ratio $f = F_s/F_d$, the MT desorption constant $K = \epsilon_0/\pi_0$, and the backward-forward velocity ratio $\nu = v_B/v_F$. Depending on the values of these parameters, the cargo is in one of three possible motility states: (0), (-+), and (-0+). These states are characterized by qualitatively different motility behaviors as illustrated in Fig. 3 for three sets of parameters.

Regulation of cargo motion requires change of the motor parameters. To show the effect of parameter changes explicitly, we calculate the 'motility diagram' shown in SI Fig. 6 for the symmetric tug-of-war with $N = N_+ = N_- = 4$

¹The case of assisting force is not treated here. It needs a definition of the single motor force-velocity relation Eq. [1] also for assisting loads $F < 0$.

symmetric plus and minus motors. This is done as follows: The single-motor parameters are taken to be equal to the kinesin 1 values as given in Table 1 except for the plus and minus motor unbinding rates $\epsilon_0 = \epsilon_{0+} = \epsilon_{0-}$ and the stall forces $F_s = F_{s+} = F_{s-}$. The parameter space (ϵ_0, F_s) is then explored systematically², and for each point the maxima of the motor number probability $p(n_+, n_-)$ is calculated and the cargo motility state is determined, as described in the section 'Numerical calculations' above. When the maxima between two scanned points change, we zoom in between these points in order to determine the transition point more accurately. The lines shown in SI Fig. 6 consist of these points at which the locations of the maxima change.

For large desorption constants K , the motors have a low affinity to the MT; therefore the number of bound motors in SI Fig. 6 is low for low K . For very high desorption constants K larger than the number of motors $N = 4$, the cargo is 'unbound', i.e. the maximum of the motor number probability is at $(\tilde{n}_+, \tilde{n}_-) = (0, 0)$. For small force ratios f , the probability distribution $p(n_+, n_-)$ has a single maximum at a state (\tilde{n}, \tilde{n}) with an equal number $\tilde{n} = \tilde{n}_+ = \tilde{n}_-$ of active plus and minus motors and is in the no-motion motility state (0) (green). For large force ratios f , the motors can generate forces large enough to rip off opposing motors since the stall force is large compared to the detachment force. This leads to the unbinding cascade described in the main text, and the motor number probability has maxima at states with only one active motor type, i.e. at $(\tilde{n}_+, 0)$ with only active plus motors and at $(0, \tilde{n}_-)$ with only active minus motors. In the latter situation, the cargo is in the $(-+)$ motility state (yellow). For intermediate values of f , both types of maxima coexist, and the cargo is in the $(-0+)$ motility state (red).

The lines in SI Fig. 6 that separate regions of different color mark the parameter sets where maxima of the motor number appear or disappear and correspond to bifurcation lines. For example, when passing from the cross labeled A in the (0) regime with a maximum at $(\tilde{n}_+, \tilde{n}_-) = (3, 3)$, corresponding to no motion, into the $(-0+)$ regime by increasing the force ratio f , two new maxima at $(\tilde{n}_+, \tilde{n}_-) = (4, 0)$ and $(\tilde{n}_+, \tilde{n}_-) = (0, 4)$ appear. This means that the cargo now exhibits fast plus and minus motion. However, this fast motion is rarely observed since the two new maxima have less probability than the pause-maximum at (3,3). With further increase of f , the maxima at (4,0) and (0,4) grow, while the maximum at (3,3) shifts to (2,2) and diminishes. Cargo motion becomes more and more dominated by fast plus and minus motion, and pauses become less frequent until they finally disappear together with the maximum at (2,2) when passing the line to the $(-+)$ regime. At the cross labeled C in SI Fig. 6, the cargo switches between fast plus and minus motion. A direct transition from the (0) to the $(-+)$ regime (without passing the $(-0+)$ regime) occurs only for maxima with low motor numbers, when the no-motion maximum and the two fast motion maxima are neighbours (either direct or diagonal) on the discrete state space (n_+, n_-) . This happens, for example, when passing from a region with a maximum at $(\tilde{n}, \tilde{n}) = (1, 1)$ to a region with maxima at $(\tilde{n}, 0) = (1, 0)$ and $(0, \tilde{n}) = (0, 1)$. The bifurcation line then marks the parameter set where all maxima have the same probability.

We investigated the average times between direction reversals in the $(-+)$ motility state and found it to grow exponen-

tially with the motor number. This indicates that the transitions between the different motility states become nonequilibrium phase transitions in the limit of large motor numbers.

SI Fig. 7 shows the motility diagram for the tug-of-war of $N_+ = 6$ plus against $N_- = 6$ minus motors with parameters closely related to the *Drosophila* lipid-droplet transport in wild type phase II. The diagram does not show maxima locations but only the bifurcation lines between the different motility states. It is generated in a similar way as SI Fig. 6: The single-motor parameters correspond to the values of the *Drosophila* plus motor kin? and dynein as given in Table 1 except for the minus motor unbinding rate ϵ_{0-} and stall force F_{s-} . The parameter space (ϵ_{0-}, F_{s-}) is then explored systematically in the same way as for the symmetric case. SI Fig. 7 exhibits seven motility states. The 'new' motility states (+), (-), (0+) and (-0) are asymmetric with respect to plus and minus motors and, thus, were not present for the symmetric tug-of-war. SI Fig. 7 shows that minus motors with high affinity to the MT, i.e. with low desorption constant K_- , favor minus motion. A high force ratio f_- enhances the unbinding cascade that leads to fast motion in the plus and/or minus direction. Minus motors with high MT affinity but low force ratio tend to block motion and lead to pauses. The irregular shape of the bifurcation lines between the motility states is a discretization effect and corresponds to transitions between different locations of the maxima of the motor number probability p , similar to the changes of maxima locations shown in SI Fig. 6.

Fit to the lipid-droplet data. We applied our tug-of-war model to the bidirectional transport of lipid-droplets in *Drosophila* embryos as studied experimentally in [8, 9, 10]. Various transport characteristics were measured in two different embryonic phases (labeled wild type phase II and III, Wt II and Wt III) and three different dynein mutation backgrounds (labeled $Dhc^{6-10}/+$, $Dhc^{8-1}/+$ and Dhc^{8-1}/Dhc^{6-10}) during phase II.

We first considered the Wt II data. From cargo stall force measurements, the experimenters concluded that the droplets are pulled in the plus and minus direction by five plus and five minus motors, respectively. Since the number of active motor fluctuates stochastically, these numbers represent the average number of pulling motors. We therefore chose the total number of plus and minus motors to be $N_+ = N_- = 6$. The droplets are transported by dynein [9] and an unknown plus motor which we call kin?. The single motor parameters of dynein are only partly known, and for the stall force different labs have reported different results, see Table 1. In the droplet experiments, cargo stall force measurements indicate a single motor stall force of 1.1 pN for both plus and minus motors³ [8]. We used this value for the stall forces of both motors and varied the remaining 10 single motor parameters $F_{d\pm}$, $\epsilon_{0\pm}$, $\pi_{0\pm}$, $v_{F\pm}$ and $v_{B\pm}$ in order to fit the experimental data.

We generated and analyzed cargo trajectories as described above in the section 'Numerical calculations'. In particular,

²All other single-motor parameters are kept constant. However, as far as backward motion is concerned, not the backward velocity v_B is kept constant but rather the backward slope v_B/F_s of the force-velocity curve, with F_s equal to the kinesin 1 value.

³For dynein, this value is in agreement with the stall force reported by [13]. The low stall force for the unknown plus motor implies that this motor should be different from kinesin 1 because the kinesin 1 stall force is 6 pN.

⁴The spatial resolution in the experiments is of the order of nanometers and therefore unproblematic.

we used the experimental time resolution⁴ and definition of runs and pauses, including the experimental cutoffs. The choice of the time resolution and the cutoffs is crucial since they strongly affect the magnitude of average run lengths, velocities or pauses. For example, short runs or pauses, which are easily accessible in simulations, may be unobservable in experiments because they are below time resolution or buried in noise. For the experimental determination of plus and minus droplet stall forces, the droplets had to be moving in a given direction 'for a few seconds' in order to decide their direction before the measurement was performed [8, 9]. We therefore averaged stall force values, calculated according to Eq. [12], only over 'very long' runs that last more than 3 s. The experiments distinguished pauses after plus and after minus runs. We adopted this distinction although both in the experiments and in our simulations both types of pauses are very similar, see below. Furthermore, the experimenters defined 'short runs' of length 30-100 nm and 'long runs' of length 500-1000 nm, and calculated average velocities of both types of runs. We followed this procedure.

For fitting, we compared 10 transport characteristics, namely plus and minus run lengths, plus and minus stall forces, pause times after plus and minus travel, and plus and minus velocities of short and long runs⁵ as shown in SI Table 3. For this purpose, we defined a 'distance function' between model and experiment as the sum of squared differences between the experimentally measured and simulated quantities. As the different quantities are of different order of magnitude, they were rescaled in such a way that the experimental values are of order unity. We then minimized this distance function with respect to the unknown model parameters.

For the Wt II fit, these are the 10 unknown single motor parameters listed above. We first chose 'reasonable' set of parameters. Here 'reasonable' means that the motor parameters must be of the order of magnitude of experimental single-motor parameters and that the simulation results must be of the order of magnitude of the experimental results. We then used the Nelder-Mead downhill simplex algorithm [14] to minimize the distance function starting from this initial choice. As this is only a local minimum, we repeated this procedure for several starting parameter sets until we found a minimum that reproduces the experimental data within about 10%.

In wild type phase III (Wt III), reduced stall forces led to the conclusion that the average number of motors pulling the cargo in both directions is only four motors. We therefore took the total number of motors on the cargo to be $N_+ = N_- = 5$. For the Wt III fit, the single-motor parameters were set to the Wt II values. Then the simplex algorithm was started from this parameter set to minimize the 'distance function' with the Wt III experimental values.

For the dynein mutation fits, only the six minus motor parameters F_{s-} , F_{d-} , ϵ_{0-} , π_{0-} , v_{F-} , v_{B-} were used as fitting parameters because the mutation only affects the dyneins, and does so in an unknown way. The plus motor parameters were kept fixed at the values from the Wt II fit since droplet motion in the dynein mutation background were investigated in embryonic phase II.

The single motor parameters resulting from all these fits are shown in SI Table 2 (the Wt II values are also shown in Table 1). They are within the expected range of motor pa-

rameters. The unbinding and binding rates are of the order of 1 s^{-1} as measured for motors like kinesin 1 [15, 16, 17] and kinesin 3 [18]. For dynein, the unbinding and binding rates lie in the experimental range [19, 13, 20]. The forward velocities are of the order of $0.5 \mu\text{m/s}$ which is close to the droplet velocity measured during long runs. This means that the tug-of-war does not substantially reduce the single-motor velocity. The backward velocity is two orders of magnitude smaller than the forward velocity but one order of magnitude larger than the kinesin 1 backward velocity. For dynein, this is in agreement with experiments [13, 21]. The wild type detachment forces obtained from the fit are approximately half of the stall force, similar as for kinesin 1, for which however both force scales are larger, see Table 1.

A comparison of the experimental data and the corresponding fit result simulation data is shown in SI Table 3. They all agree within 10%.

A remarkable feature of droplet transport is the positive correlation of run length and velocity, see Fig. 5B: longer runs have larger velocities. The correlation persists when considering run times and velocities instead, see SI Fig. 8A. This is more meaningful since run length and velocity are trivially linearly correlated due to the fact that high velocities lead to larger displacement. As explained in the main text, the correlation is caused via a correlation of the average number of active winning motors with the run length, see SI Fig. 8B. In the experiments, the correlation has been quantified by dividing the runs into short and long runs as defined above and comparing the average velocities of these runs. For visual comparison, both model and experimental results are shown in SI Fig. 9.

Although not used in the fitting procedure, the distributions of run length and of pause time show the same qualitative and similar quantitative behavior in simulation and experiment. Fig. 5A and SI Fig. 10 show the plus and minus run length distributions for all genotypes in wild type phase II, which can all be fitted by a double exponential function. The same behavior was found in the experiments [10]. The short and long decay lengths of these fits are listed in SI Table 4. The short decay lengths are ca. $0.1 \mu\text{m}$, while the long decay lengths are of the order of $1 \mu\text{m}$ and vary in the different genetic backgrounds. Although not used for fitting, simulation and experimental values are of the same order of magnitude and agree within 50%.

SI Fig. 11 shows the pause time distribution for Wt II parameters. We did not distinguish pauses after plus and minus runs here because they were statistically indistinguishable. The pause time distribution can be fitted by a single exponential distribution with the time scale 0.38 s. All this is also found for the experimental distributions of pauses after plus and after minus runs, which are very similar to each other and can be fitted with a single exponential function with the time scales 0.24 s and 0.29 s, respectively [9].

The agreement of simulation and experiment shows that our tug-of-war model can describe the lipid-droplet data. Two features are particularly remarkable because they are not ex-

⁵We did not use quantities that are extremely sensitive to the detectability of pauses, such as the percentage of direction reversals associated with pauses, or the average time between pauses, because pauses in simulation are more readily detected than in experiment. We also did not use 'secondary' quantities that were obtained by further processing of the data, such as fits to run length or pause time distributions or quantities calculated from these fits.

pected within a naive picture of a tug-of-war: First, the Wt II and Wt III data represent motion with balanced stall forces in plus and minus direction, but the motion is net plus end-directed in phase II and net minus-end directed in phase III. Second, the dynein mutation data, which exhibit an impairment of both plus and minus motion, could be reproduced by varying the dynein single-motor parameters only. Both observations are in agreement with our tug-of-war model, as shown by the successful fit. The reason is that in our model cargo motion depends on six different motor properties (stall and detachment force, binding and unbinding rate, and forward

and backward velocity) for each motor type, which leads to a rather complex behavior. In particular, cargo motion is not only determined by the motor forces but also by other motor properties, which leads to a variable response to perturbations such as mutation or regulation. As shown in SI Table 3, it is possible (i) to change only one direction and leave the other direction unaffected (Wt III, or change of only minus motor stall force or forward or backward velocity) (ii) to impair one direction and enhance the other (change of only minus motor unbinding or binding rate or detachment force), or (iii) to impair both directions (dynein mutations).

1. Svoboda K, Block SM (1994) *Cell* 77: 773–784.
2. Kojima H, Muto E, Higuchi H, Yanagida T (1997) *Biophys J* 73: 2012–2022.
3. Visscher K, Schnitzer MJ, Block, SM (1999) *Nature* 400: 184–189.
4. Toba S, Watanabe TM, Yamaguchi-Okimoto L, Toyoshima YY, Higuchi H (2006) *Proc Natl Acad Sci USA* 103: 5741–5745.
5. Carter NJ, Cross RA (2005) *Nature* 435: 308–312.
6. Klumpp S, Lipowsky R (2005) *Proc Natl Acad Sci USA* 102: 17284–17289.
7. Mallik R, Gross SP (2004) *Curr Biol* 14: R971–R982.
8. Welte MA, Gross SP, Postner M, Block, SM, Wieschaus EF (1998) *Cell* 92: 547–557.
9. Gross SP, Welte MA, Block SM, Wieschaus EF (2000) *J Cell Biol* 148: 945–955.
10. Gross SP, Welte MA, Block SM, Wieschaus EF (2002) *J Cell Biol* 156: 715–724.
11. vanKampen NG (1992) *Stochastic processes in physics and chemistry* (Elsevier, Amsterdam).
12. Gillespie DT (1976) *J Comp Phys* 22: 403–434.
13. Mallik R, Petrov D, Lex SA, King SJ, Gross SP (2005) *Nature* 427: 649–652.
14. Press WH, Teukolsky SA, Vetterling WT, Flannery BP (2002) *Numerical recipes in C++ : the art of scientific computing* (Cambridge: Cambridge University Press, New York).
15. Vale RD, Funatsu TS, Pierce DW, Romberg L, Harada Y, Yanagida T (1996) *Nature* 380: 451–453.
16. Schnitzer MJ, Visscher K, Block SM (2000) *Nature Cell Biol* 2: 718–723.
17. Leduc C, Campas O, Zeldovich KB, Roux A, Jolimaître P, Bourel-Bonnet L, Goud B, Joanny J-F, Bassereau P, Prost J (2004) *Proc Natl Acad Sci USA* 101:17096–17101.
18. Tomishige M, Vale RD (2002) *Science* 297: 2263–2267.
19. King SJ, Schroer TA (2000) *Nature Cell Biol* 2: 20–24.
20. Reck-Peterson SL, Yildiz A, Carter AP, Gennerich A, Zhang N, Vale RD (2006) *Cell* 126:335–348.
21. Wang Z, Khan S, Sheetz MP (1995) *Biophys J* 69: 2011–2023.

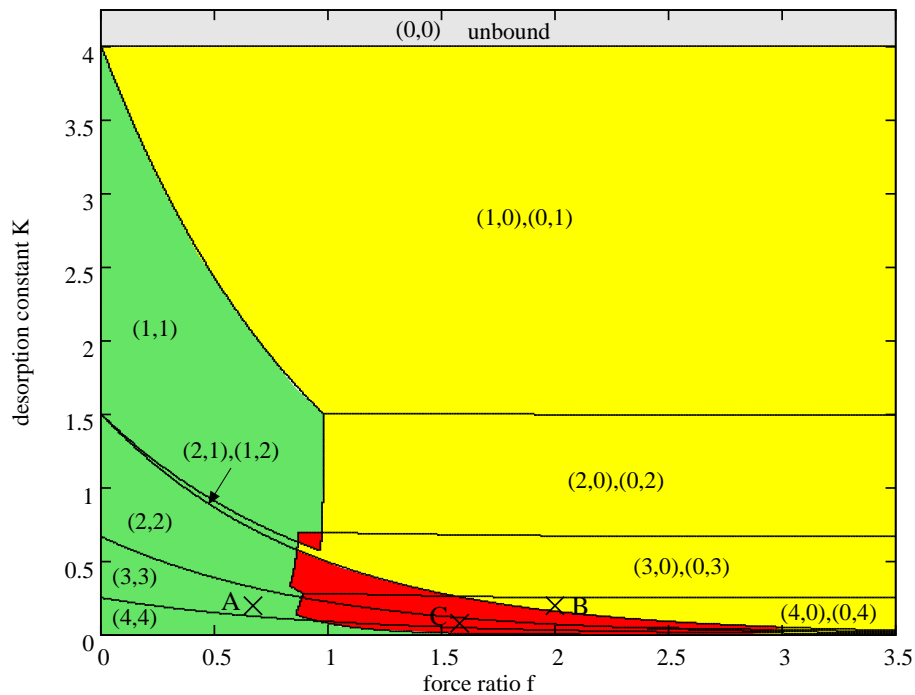


Fig. 6. Motility diagram for the tug-of-war of $N_+ = N_- = 4$ symmetric plus and minus motors with identical single-motor parameters but different forward directions. Depending on the motor force ratio $f = F_s/F_d$ of the stall and the detachment force and the MT desorption constant $K = \epsilon_0/\pi_0$, the cargo transport exhibits three different motility regimes denoted by (0), $(-+)$, and $(-0+)$. These regimes are defined via the number and locations of the maxima of the motor number probability distribution $p(n_+, n_-)$ as described in the text. The lines in the motility diagram separate regions in which the maxima of the probability distribution are located at different motor number states. The colors separate regions with different motility states. In motility state (0) (green) the motor number distribution has a single maximum at a no-motion state with an equal number of plus and minus motors bound at (\tilde{n}, \tilde{n}) with $1 \leq \tilde{n} \leq 4$. The two near-diagonal maxima at (1,2) and (2,1) are also counted as a single diagonal maximum, which in a continuous state space would be at (\tilde{n}, \tilde{n}) with $1 < \tilde{n} < 2$. If the maximum is at $(\tilde{n}, \tilde{n}) = (0,0)$ the cargo is considered as 'unbound' (gray). In the $(-+)$ regime (yellow), the probability distribution exhibits two maxima with only plus or only minus motors bound at $(\tilde{n}, 0)$ and $(0, \tilde{n})$ with $1 \leq \tilde{n} \leq 4$. The cargo is in the $(-0+)$ regime (red) if the probability distribution exhibits three maxima. The parameters are kinesin-like as in Table 1 except for the stall force F_s and the unbinding rate ϵ_0 , which are varied. The crosses labeled A, B and C mark the parameter sets for the cargo trajectories, probability and velocity distributions shown in the corresponding Fig. 3A-C, which illustrate the qualitatively different motility behaviours for the different motility regimes. The cross B in the $(-+)$ regime corresponds to the complete set of kinesin parameters with $f = 6/3$ and $K = 1/5$, while A in the (0) regime is at $f = 2/3$ and $K = 1/5$ and C in the $(-0+)$ regime is at $4.75/3$ and $K = 0.4/5$.

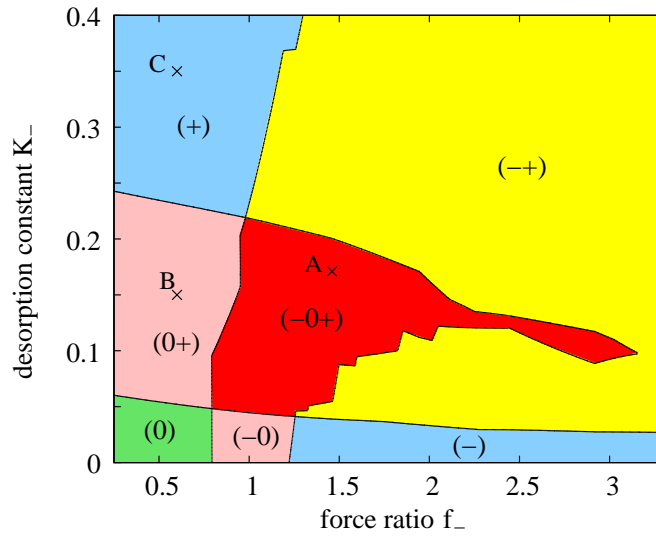


Fig. 7. Motility diagram for the asymmetric tug-of-war of $N_+ = 6$ plus against $N_- = 6$ minus motors related to the *Drosophila* lipid-droplet transport. Plus and minus motor parameters are for the *Drosophila* plus motor (kin?) and dynein, respectively, as in Table 1 except for the stall force F_{s-} and the detachment rate ϵ_{0-} of the minus motors which are varied. Depending on the minus motor force ratio $f_- = F_{s-}/F_{d-}$ and the MT desorption constant $K_- = \epsilon_{0-}/\pi_{0-}$, the cargo exhibits seven different motility regimes: no motion (0), fast plus motion (+), fast minus motion (-), coexistence between two of these states as indicated by (0+), (-0), and (-+), and three-state coexistence (-0+). The motility states are defined via the maxima of the motor number probability distribution $p(n_+, n_-)$. Plus motion (+) corresponds to a maximum at $(\tilde{n}_+, 0)$ with only plus motors active, minus motion (-) to a maximum at $(0, \tilde{n}_-)$ with only minus motors active, and no motion (0) to a maximum at $(\tilde{n}_+, \tilde{n}_-)$ with both motor types active. The other motility states exhibit the combinations of these maxima as indicated by the notation. For example, in the regime (0+), the probability distribution has one maximum at a plus motion state and one maximum at a no-motion state. The crosses labeled A, B and C correspond to the parameter values for Fig. 4A-C, which illustrate the qualitatively distinct motility behavior for the different motility regimes. The cross A in the (-0+) regime corresponds to the tug-of-war for *Drosophila* droplet transport in wild type phase II with parameters as given in Table 1. The cross B in the (0+) regime is at $f_- = 0.60$ and $K_- = 0.15$, and C in the (+) regime at $f_- = 0.60$ and $K_- = 0.34$.

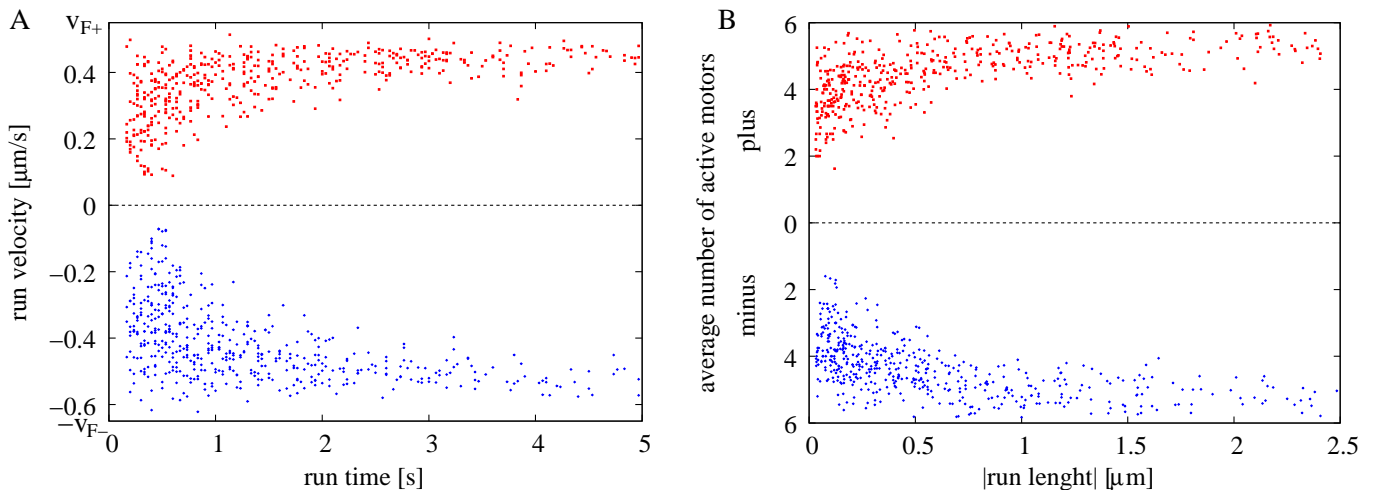


Fig. 8. Scatter plots (A) of run velocities against run times and (B) of average number of active plus resp. minus motors against absolute run lengths for the *Drosophila* droplet tug-of-war in wild type phase II for 500 runs in each direction, divided up into the positive plus runs (red) and the negative minus runs (blue). (A) The absolute run velocities are larger for longer runs and almost reach their maximal values of the single motor velocities $v_{F+} = 0.55 \mu\text{m/s}$ and $v_{F-} = 0.65 \mu\text{m/s}$ for very long runs. This shows that the correlation of run length and velocity discussed in the main text persists when considering run times and velocities instead. This is more meaningful since run length and velocity are trivially linearly correlated due to the fact that high velocities lead to larger displacement. (B) The reason for the correlation is that longer runs also have a higher average number of active pulling motors, compare the discussion in the main text. There are no data points for small run times, lengths and velocities because runs have been defined as having a velocity of at least 50 nm/s for at least 30 nm and 0.16 s .

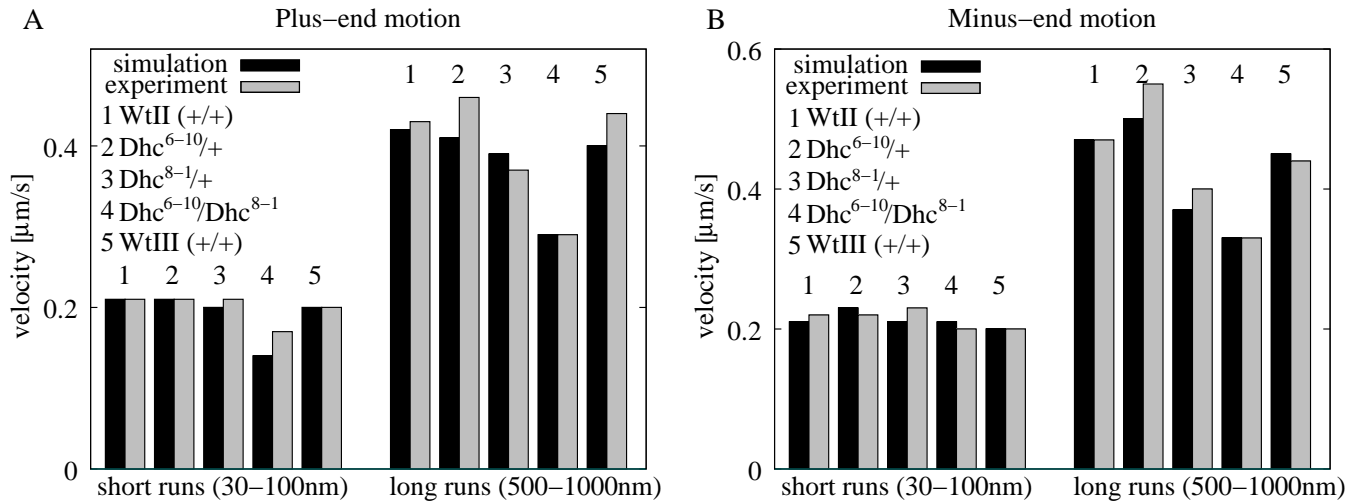


Fig. 9. Mean run velocity for short (30-100 nm) and long (500-1000 nm) runs for different *Drosophila* embryonic phases (Wt II and Wt III) and dynein mutations (*Dhc*^{6-10/+}, *Dhc*^{8-1/+} and *Dhc*^{8-1/Dhc}⁶⁻¹⁰) for (A) plus-end motion and (B) minus-end motion. Short runs have shorter velocities than long runs, and changes for the different phases or genotypes are via the velocity of the long runs. The simulations values (black) are taken from SI Table 3 and agree well with the experimental values (gray), which are read off from Fig. 4 in Ref. [10] and Fig. 7 in Ref. [9].

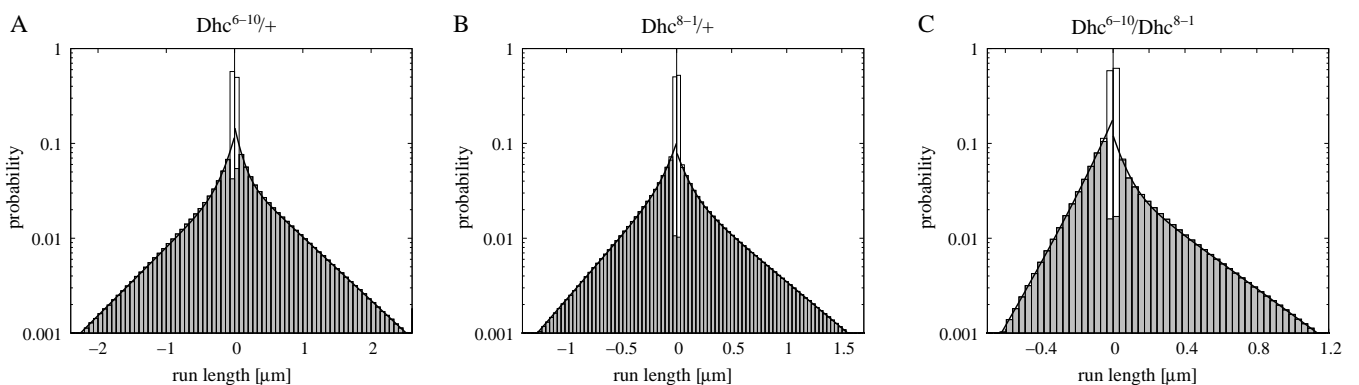


Fig. 10. Run length distributions for three different dynein mutations labeled (A) *Dhc*^{6-10/+}, (B) *Dhc*^{8-1/+}, and (C) *Dhc*^{8-1/Dhc}⁶⁻¹⁰. Plus (minus) run lengths are positive (negative). In all cases, the run length distribution can be fitted by a double exponential function corresponding to the solid line. The single motor parameters of the corresponding simulations are given in SI Table 2. The two decay lengths of the double-exponential fits are listed in SI Table 4.

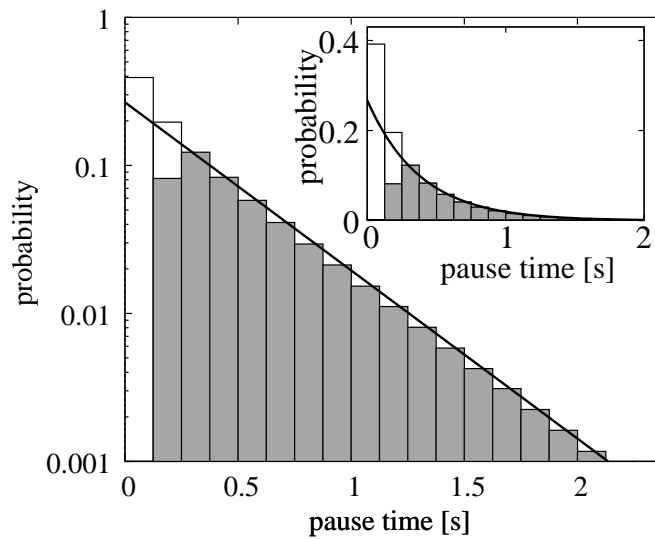


Fig. 11. The pause time distribution (gray histogram) for the tug-of-war with wild type phase II parameters can be fitted by a single exponential distribution (line) with time scale 0.38 s. We did not distinguish pauses after plus and after minus motion because they are statistically indistinguishable. The full graph is a semi-logarithmic plot of the original distribution shown in the inset. The first bar has reduced counts because of the experimental definition of a pause to be longer than 0.23 s. The distribution looks similar to the experimental distributions of pauses after plus and after minus motion in Fig. 5 of Ref. [9], which have been fitted with single-exponential distributions with time scales 0.24 s and 0.29 s. These time scales are smaller than the experimental average pause times of 0.55 s for pauses after plus and 0.62 s for pauses after minus motion. Similarly, in simulation, the time scale 0.39 s of the exponential fit is smaller than the average pause time of 0.61 s. This indicates that the distribution is in fact not single exponential but has another, smaller time scale. This smaller time scale is below experimental resolution and shows up only when the experimental lower time cutoff 0.23 s for the pauses is removed (white histogram).

Table 2. Single-motor parameters for the fits to *Drosophila* lipid-droplet transport in wild type phase II (Wt II) and III (Wt III), and for three different dynein mutations ($Dhc^{6-10}/+$, $Dhc^{8-1}/+$, and Dhc^{8-1}/Dhc^{6-10}). The motor numbers are $N_+ = N_- = 6$ except for Wt III with $N_+ = N_- = 5$. The plus motor parameters for the dynein mutations are as for the plus motors in Wt II.

Motor direction	Wt II		$Dhc^{6-10}/+$	$Dhc^{8-1}/+$	Dhc^{8-1}/Dhc^{6-10}	Wt III	
	plus	minus	minus	minus	minus	plus	minus
stall force F_s [pN]	1.1	1.1	1.1	1.1	0.85	1.1	1.1
detachment force F_d [pN]	0.82	0.75	0.88	0.84	1.1	0.82	0.81
unbinding rate ϵ_0 [s^{-1}]	0.26	0.27	0.45	0.37	0.54	0.26	0.27
binding rate π_0 [s^{-1}]	1.6	1.6	1.8	2.0	1.8	1.4	1.6
forward velocity v_F [$\mu m/s$]	0.55	0.65	0.69	0.49	0.44	0.56	0.63
back velocity v_B [nm/s]	67	72	77	76	53	68	73

Table 3. Mutation and regulation in lipid-droplet transport: results of the fit to the *Drosophila* lipid-droplet data. The first 10 lines show a comparison of the average plus and minus stall forces, the average plus and minus run lengths, the average times of pauses after plus and after minus runs, and the average velocities of short and long runs in plus and in minus direction as obtained in simulation (sim.) and experiment* (exp.) for wild type phase II (Wt II) and III (Wt III), and for three different dynein mutations ($Dhc^{6-10}/+$, $Dhc^{8-1}/+$, and Dhc^{8-1}/Dhc^{6-10}). The last column describes the net effect on motion (run lengths and velocities) as compared to the Wt II values. The last seven lines show the effect of a change of one single motor parameter from the Wt II value, given in front of the arrow, to the value given after the arrow in the first column.

	average stall force [pN]		average run length [μm]		average pause time after [s]		average velocity [$\mu m/s$]				net effect on motion plus/minus
	plus	minus	plus	minus	plus	minus	short runs		long runs		
							plus	minus	plus	minus	
Wt II (sim.)	5.4	5.3	0.84	0.66	0.61	0.61	0.21	0.21	0.42	0.47	-/-
Wt II (exp.)	5.5	5.5	0.84	0.62	0.55	0.62	0.21	0.22	0.43	0.47	
$Dhc^{6-10}/+$ (sim.)	5.2	5.0	0.58	0.53	0.54	0.54	0.21	0.23	0.41	0.50	impaired/impaired
$Dhc^{6-10}/+$ (exp.)	5.5	5.5	0.56	0.49	0.60	0.62	0.21	0.22	0.46	0.55	
$Dhc^{8-1}/+$ (sim.)	5.3	5.1	0.41	0.32	0.66	0.66	0.20	0.21	0.39	0.37	impaired/impaired
$Dhc^{8-1}/+$ (exp.)	5.1	5.5	0.38	0.29	0.71	0.70	0.21	0.23	0.37	0.40	
Dhc^{8-1}/Dhc^{6-10} (sim.)	5.0	3.9	0.29	0.15	0.71	0.75	0.14	0.21	0.29	0.33	impaired/impaired
Dhc^{8-1}/Dhc^{6-10} (exp.)	4.7	3.7	0.31	0.17	0.71	0.76	0.17	0.20	0.29	0.33	
Wt III (sim.)	4.3	4.4	0.42	0.60	0.59	0.59	0.20	0.20	0.40	0.45	impaired/-
Wt III (exp.)	4.4	4.4	0.42	0.60	-	0.60	-	0.20	-	0.44	
$F_{s-} = 1.1$ pN \rightarrow 0.8 pN	5.3	3.9	0.83	0.25	0.75	0.83	0.16	0.24	0.39	0.47	-/impaired
$F_{d-} = 0.75$ pN \rightarrow 1.0 pN	4.9	5.3	0.24	0.80	0.74	0.73	0.14	0.20	0.35	0.47	impaired/enhanced
$\epsilon_{0-} = 0.27$ s^{-1} \rightarrow 0.5 s^{-1}	5.5	4.9	2.0	0.35	0.44	0.45	0.27	0.23	0.45	0.48	enhanced/impaired
$\pi_{0-} = 1.6$ s^{-1} \rightarrow 2.5 s^{-1}	5.4	5.5	0.35	0.97	0.67	0.65	0.22	0.20	0.40	0.48	impaired/enhanced
$v_{F-} = 0.65$ $\frac{\mu m}{s}$ \rightarrow 1.0 $\frac{\mu m}{s}$	5.3	5.4	0.85	1.4	0.59	0.60	0.21	0.24	0.42	0.70	-/enhanced
$v_{B-} = 72$ $\frac{nm}{s}$ \rightarrow 6.0 $\frac{nm}{s}$	5.8	5.3	2.1	0.65	0.63	0.66	0.43	0.21	0.52	0.47	enhanced/-
$N_- = 6$ \rightarrow $N_- = 5$	5.3	4.4	1.3	0.37	0.55	0.58	0.21	0.22	0.42	0.46	enhanced/impaired

*The experimental values are taken from [8, 9, 10] as follows: The average stall forces for Wt II and Wt III are directly given in [8]; the other stall forces are read off from the diagrams in Fig. 3 in [9] and Fig. 2, 3 in [10] by applying the procedure described in the experimental procedures of [8]. The average run lengths are from Tab. II in [9] and Tab. I in [10], the average pause times from Tab. I in [9] and Tab. II in [10]. The average velocities for short and long runs have been read off from histograms in Fig. 7 in [9] and Fig. 4 in [10]. Missing values were not available.

Table 4. Mutation and regulation in lipid-droplet transport: results of the fit to the *Drosophila* lipid-droplet data that have not been used in the fitting procedure. In all phases and genetic backgrounds, the run length distributions can be fitted by a double exponential function, see Fig. 5A and SI Fig. 10 with the short and long decay lengths given here. Although not used for fitting, the simulation and experimental* values are of the same order of magnitude; the maximal error is 50%.

	decay lengths [μm]			
	short		long	
	plus	minus	plus	minus
Wt II (sim.)	0.099	0.13	0.95	0.80
Wt II (exp.)	0.067	0.098	1.1	1.1
<i>Dhc</i> ⁶⁻¹⁰ /+ (sim.)	0.010	0.13	0.65	0.61
<i>Dhc</i> ⁶⁻¹⁰ /+ (exp.)	0.088	0.10	0.78	0.90
<i>Dhc</i> ⁸⁻¹ /+ (sim.)	0.094	0.083	0.45	0.33
<i>Dhc</i> ⁸⁻¹ /+ (exp.)	0.074	0.091	0.40	0.65
<i>Dhc</i> ⁸⁻¹ / <i>Dhc</i> ⁶⁻¹⁰ (sim.)	0.059	0.079	0.31	0.14
<i>Dhc</i> ⁸⁻¹ / <i>Dhc</i> ⁶⁻¹⁰ (exp.)	0.052	0.044	0.44	0.21
Wt III (sim.)	0.13	0.14	0.48	0.67
Wt III (exp.)	0.096	0.083	0.78	1.1

*The experimental decay length values are from Tab. I in [10], and Tab. II in [9].